Investigation of Coupling Tuning in Self-Coupled Optical Waveguide Resonators

Xiaomeng Sun, Linjie Zhou, *Member, IEEE*, Jingya Xie, Zhi Zou, Liangjun Lu, Haike Zhu, Xinwan Li, *Senior Member, IEEE*, and Jianping Chen

***Abstract*— We investigate the influence of coupling strength on self-coupled optical waveguide (SCOW) resonators. Experimental results reveal that the SCOW resonator transmission spectrum can exhibit single-channel or dual-channel stopbands with the band splitting level determined by the two coupling coefficients. Electrically tunable SCOW resonators comprising 2 × 2 Mach-Zehnder interferometer couplers are also demonstrated, which shows a similar change trend upon coupling tuning.**

***Index Terms*— Integrated optoelectronics, optical resonators, optoelectronic devices.**

I. Introduction

AFTER dominating the electronics industry for decades, silicon is on the verge becoming the material of choice for the photonics industry. Silicon photonics is one of the most promising candidates for realization of very large scale integration (VLSI) of photonic devices [1]. A key building block for VLSI photonic circuits is the micro-resonators due to their compact size and agile functionality, which have found wide applications in optical filtering/add-drop multiplexing [2], [3], bio-sensing [4], [5], and signal processing [6], [7]. On the other hand, single-channel, dual-channel, or broad-stopband notch filters with a high extinction ratio could be useful. A waveguide-coupled microring resonator can work as a single-channel notch filter. To get a high extinction ratio, the critical coupling condition should be satisfied, imposing a great challenge on device fabrication. Mode mutual coupling enabled by sidewall scattering in microring resonators could induce resonance splitting, leading to dual-channel or broad-stopband notch filters [8], [9]. However, the splitting level is very hard to control, especially given the nano-scale grating on the sidewall. Cascaded and concentric microring resonators can be used to generate high-order notch filters [9], [10] However, the resonance frequencies for all resonators should be accurately aligned, challenging for device fabrication.

Previously we proposed a novel self-coupled optical waveguide (SCOW) resonator to generate unique resonance features [11]–[13]. Unlike conventional coupled microring resonators, SCOW resonators have their clockwise and counter-clockwise resonance modes co-excited, leading to distinct resonance spectrum. The transmission behavior of SCOW resonators is quite dependent on the coupling coefficients as discussed in our previous work. In this letter, we investigate in detail the influence of coupling coefficients on SCOW resonances. Our experimental results show that the SCOW resonators can exhibit single-channel, dual-channel, or broad-stopband filtering features depending on the coupling coefficients. Based on the characterization of passive SCOW resonators, we also implement an active SCOW resonator with its coupling coefficients being electrically tunable using p-i-n diodes. The active device exhibits a similar change trend in its transmission spectrum with the tuning of coupling.

II. Passive SCOW Resonators With Varied Coupling

Fig. 1(a) shows the scanning electron microscope (SEM) image of one of the fabricated passive SCOW resonators. These devices were fabricated on a silicon-on-insulator (SOI) substrate with a 220 nm thick top silicon layer and a 3 μm thick buried oxide (BOX) layer using standard silicon microelectronics fabrication processes. The silicon channel waveguide is 450 nm wide and 220 nm high. Gratings are used for input and output coupling, as shown in Fig. 1(b).

Transmission measurements were performed using the Agilent loss and dispersion analyzer (86038B). The input light is transverse-electrically (TE) polarized by using a polarizer controller before the device under test.

Fig. 2(a)–(e) show the measured transmission spectra of the SCOW resonators with symmetric couplers of an equal length ($l_{c1} = l_{c2}$). The coupling gap (w_g) is fixed at 0.2 μm. The bending radii of the outer ring (r_1) and the inner bridge waveguides (r_2) are 6 μm and 12 μm, respectively. We can see that as the coupling length increases from 11 μm to 19 μm, the original two closely spaced channels gradually merges into one, while the notch extinction ratio (ER) decreases. This is because, for a short coupling length, the coupling to resonance is strong, resulting in a strong interference between two inherent resonance paths [11]. With an appropriate coupling

Manuscript received December 20, 2012; revised February 25, 2013; accepted March 27, 2013. Date of publication April 5, 2013; date of current version April 25, 2013. This work was supported in part by the 973 Program under Grant ID2011CB301700, in part by the National Natural Science Foundation of China under Grant 61007039 and Grant 61001074, and in part by the Science and Technology Commission of Shanghai Municipality under Project 10DJ1400402 and Project 12XD1406400.

The authors are with the State Key Laboratory of Advanced Optical Communication Systems and Networks, Department of Electronic Engineering, Shanghai Jiao Tong University, Shanghai 200240, China (e-mail: sunxiaomeng@sjtu.edu.cn; ljzhou@sjtu.edu.cn; xiejingya.ok@163.com; zhizou@sjtu.edu.cn; luliangjun@sjtu.edu.cn; 156027948@qq.com; lixinwan@sjtu.edu.cn; jpchen62@sjtu.edu.cn).

Color versions of one or more of the figures in this letter are available online at http://ieeexplore.ieee.org.

Digital Object Identifier 10.1109/LPT.2013.2256778

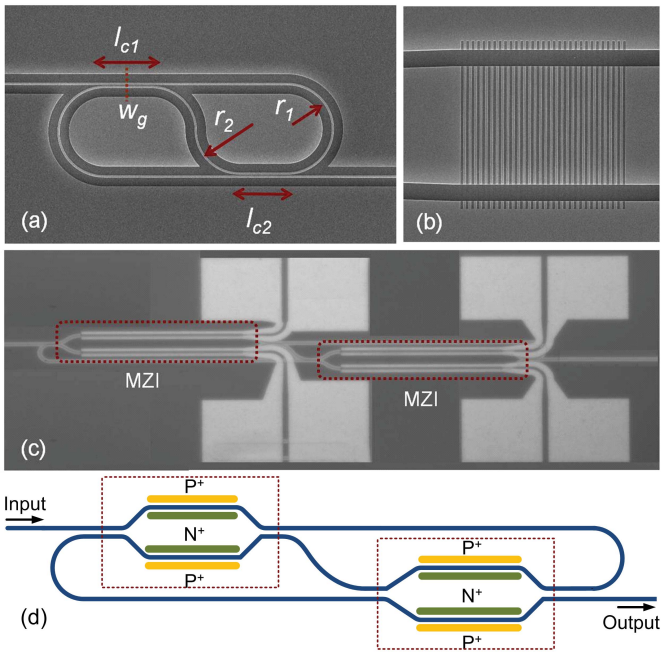

Fig. 1. SEM image of (a) fabricated SCOW resonator and (b) waveguide grating coupler. (c) Microscopic photograph of the fabricated active SCOW resonator with its couplers formed by two tunable 2 × 2 MZIs. (d) Schematic illustration of the active SCOW resonator.

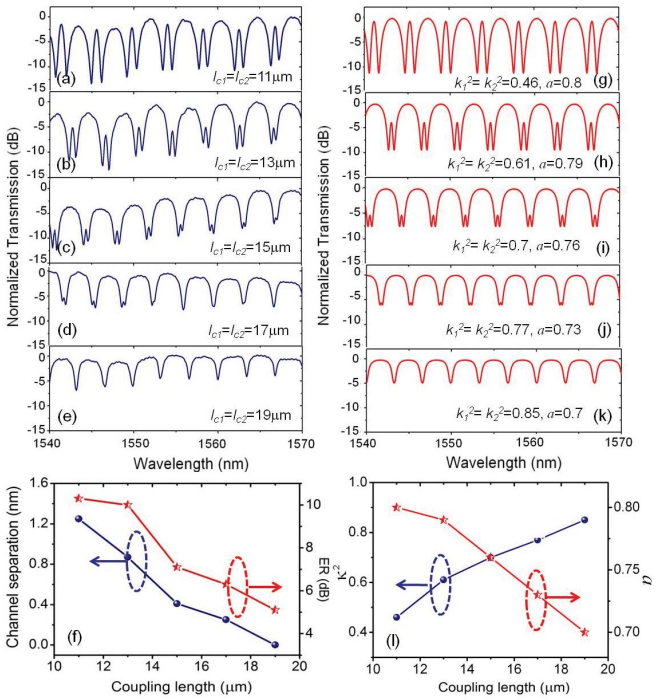

Fig. 2. Measured transmission spectra of the symmetric SCOW resonators with various coupling lengths (a) 11, (b) 13, (c) 15, (d) 17, and (e) 19 μm. (f) Measured channel separation and resonance ER versus coupling length. (g)–(k) Corresponding modeled transmission spectra. (l) Extracted coupling coefficient κ^2 and loss factor a versus coupling length.

length (∼15 μm), the notch bottom is near flat, which could be regarded as one broad stopband. Waveguide loss, which mainly comes from the waveguide linear scattering loss, plays an important role in generating the resonance spectrum. With the increase of coupling length, the central peak is gradually weakened since the loss exceeds the coupling strength. It should be noted that, if there is no loss, then there is always a sharp peak in the center. To reduce the waveguide loss, thermal oxidation process can be adopted to smooth the waveguide etched sidewalls [14].

Fig. 2(f) shows the measured dual-channel separation and resonance ER change with the coupling length around 1550 nm. The channel separation decreases from 1.25 nm at the coupling length of 11 μm to 0 at the coupling length of 19 μm, while the extinction ratio (ER) is decreased from 10.3 dB to 5.1 dB.

With the transfer matrix approach, the field transmission function of the SCOW resonator can be expressed as [11]

$$t_r = -a^{1/6}e^{-i\theta}\left[\frac{(\kappa_1-\kappa_2 a e^{-i\phi})(\kappa_2-\kappa_1 a e^{-i\phi})}{(1-\kappa_1\kappa_2 a e^{-i\phi})^2} + \left(\frac{t_1 t_2 a^{1/2}e^{-i\phi/2}}{1-\kappa_1\kappa_2 a e^{-i\phi}}\right)^2\right] \quad (1)$$

where θ and φ are the phase change associated with the bridge waveguide and the resonator round-trip, respectively, t_i and $\kappa_i (i = 1, 2)$ are the transmission and coupling coefficients of the two couplers ($t_1 = t_2$ and $\kappa_1 = \kappa_2$ for symmetric couplers), respectively, and a is the loss factor associated with the SCOW resonance. When φ satisfies $\varphi = 2m\pi$ (m is an integer), resonance occurs.

Using the theoretical modeling, we also plot the transmission spectra corresponding to various coupling coefficients as shown in Fig. 2(g)–(k). It can be seen that there is a good agreement between the theoretical and experimental results. The power coupling ratio κ^2 and loss factor a changing with the coupling length are extracted and shown in Fig. 2(l). With the increase of coupling length from 11 μm to 19 μm, κ^2 changes from 0.46 to 0.85, and a is decreased from 0.8 to 0.7. For directional couplers as used in our SCOW resonators, the power coupling ratio changes with the coupling length in a squared sinusoidal function, which explains the rising trend of the κ^2 curve. We attribute the slight decrease in a with the coupling length to the additional loss caused by the longer directional coupler.

The phase and group delay responses also affect the filtered optical signal. Based on Eq. (1), we plot the phase Φ and group delay (GD) spectra corresponding to the configurations of the above symmetric SCOW resonators as shown in Fig. 3(a)–(e) and (f)–(j), respectively. The phase Φ is obtained from the complex transmission function of Eq. (1) as $\Phi = arg(t_r)$, and the GD is given by the first order derivative of the phase with respect to angular frequency as GD $= -d\Phi/d\omega$. Interestingly, the two dips in the power transmission spectra are always connected with negative group delay, while the presence of the central peak (due to the separation of the two dips) increases the group delay to become even positive (Fig. 3(f)–(h)).

The SCOW resonator can also be configured with asymmetric coupling. Fig. 4(a) and (b) show the measured spectra of the SCOW resonators with asymmetric couplers ($l_{c1} \neq l_{c2}$). For $l_{c1} = 13$ μm and $l_{c2} = 24$ μm (the other parameters are the same with the previous devices), the destructive interference inside the SCOW resonator makes the resonance notch deeper,

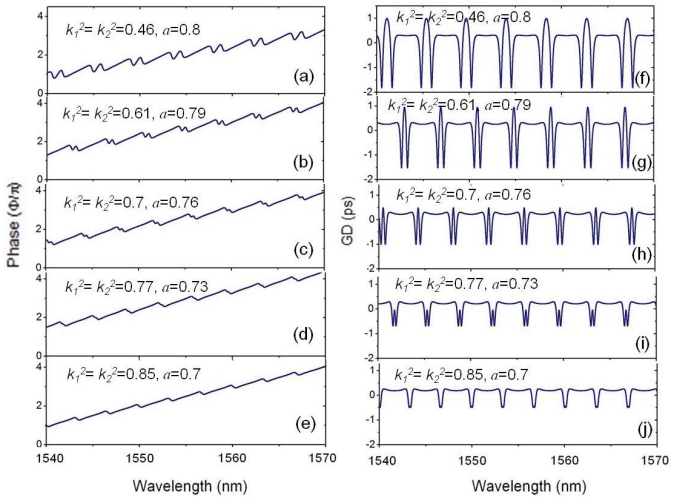

Fig. 3. (a)–(e) Modeled phase spectra of the symmetric SCOW resonators with various coupling coefficients and loss factors. (f)–(j) Corresponding GD spectra.

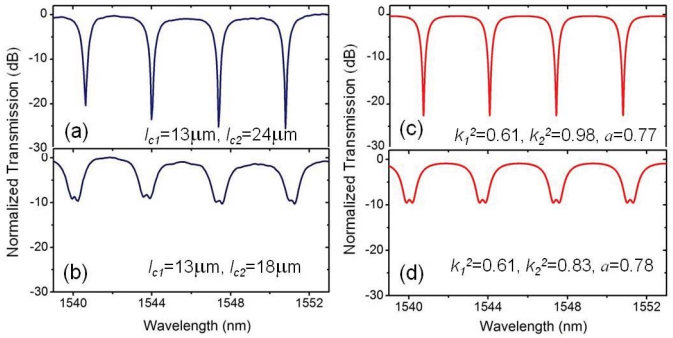

Fig. 4. Measured transmission spectra of the asymmetric SCOW resonators with coupling lengths (a) $l_{c1} = 13\ \mu$m, $l_{c2} = 24\ \mu$m and (b) $l_{c1} = 13\ \mu$m, $l_{c2} = 18\ \mu$m. (c) and (d) Corresponding modeled transmission spectra.

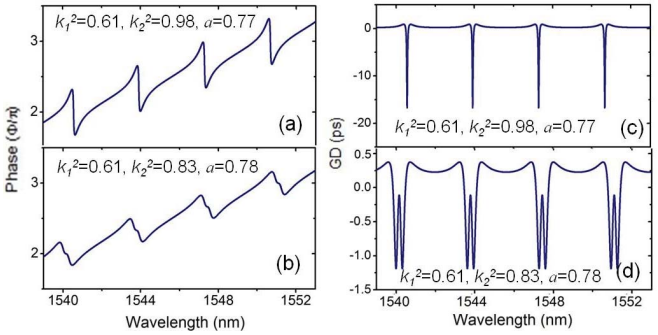

Fig. 5. (a) and (b) Modeled phase spectra of the asymmetric SCOW resonators. (c) and (d) Corresponding GD spectra.

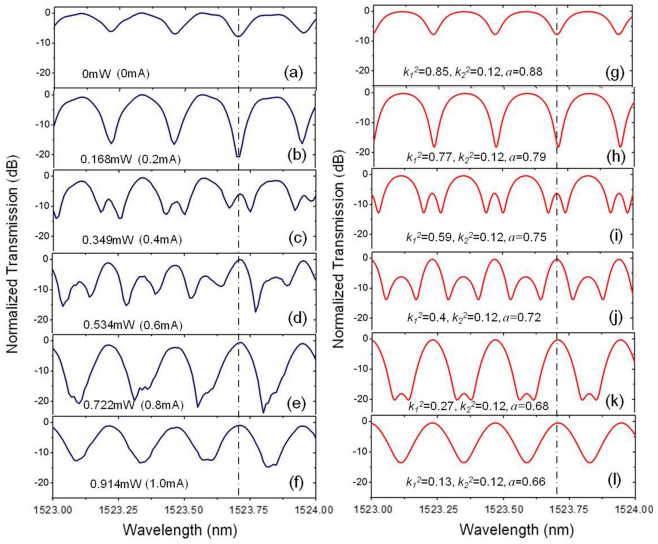

Fig. 6. Active tuning of the SCOW resonator under various electrical powers (a) 0, (b) 0.168, (c) 0.349, (d) 0.534, (e) 0.722, and (f) 0.914 mW. (g)–(l) Corresponding modeled transmission spectra.

indicating that the critical coupling is nearly reached at the resonance wavelengths, as shown in Fig. 4(a). The ER is ~26 dB around 1550 nm. Fig. 4(c) shows the modeled transmission spectrum. The κ^2 and α are extracted to be $\kappa_1^2 = 0.61$, $\kappa_2^2 = 0.98$, and $a = 0.77$. When $l_{c1} = 13\ \mu$m and $l_{c2} = 18\ \mu$m, the resonance notch is broadened and bottom flattened, as shown in Fig. 4(b). The ER is ~9.5 dB, the full-width-half-maximum (FWHM) width is ~1.2 nm, and the bottom ripple is ~0.7 dB around 1550 nm. The extracted κ^2 and α are $\kappa_1^2 = 0.61$, $\kappa_2^2 = 0.83$, and $a = 0.78$, as shown in Fig. 4(d).

Fig. 5(a) and (b) show the modeled phase spectra of the two asymmetric SCOW resonators in Fig. 4. Fig. 5(c) and (d) are their corresponding group delay spectra.

III. Electrically Tunable SCOW Resonators

To actively tune the coupling coefficients, we also designed an active SCOW resonator with the directional couplers replaced by symmetric 2 × 2 Mach-Zehnder interferometer (MZI) couplers. Phase tuning is enabled by the integrated p-i-n diode using the free-carrier plasma dispersion effect in silicon. Fig. 1(c) shows the microscope photograph of the fabricated tunable SCOW resonator. To more clearly illustrate the device structure, we also show the schematic view in Fig. 1(d). The silicon ridge waveguide dimension is 450 nm × 220 nm with a 60 nm slab. The active SCOW device is upper-clad with a 1.5 μm thick silicon dioxide. The highly doped P^+ and N^+ regions are separated by 1.65 μm to minimize the dopant absorption loss. The bending radii are $r_1 = 20\ \mu$m and $r_2 = 40\ \mu$m. The MZI active arm length is 300 μm.

The SCOW resonator is actively tuned by injection of free carriers into one of the MZI arms upon a forward bias. Fig. 6(a)–(f) show the resonance spectrum evolution with the tuning power applied on the front MZI coupler. The free spectral range (FSR) is around 0.25 nm, smaller than the former passive devices (3-4 nm). This is resulted from the longer device perimeter after the MZIs are inserted. It can be seen that, with the increment of tuning power, the spectrum changes gradually from a single-channel resonance to a dual-channel resonance with an increasing band splitting. With a power dissipation of ~0.914 mW, the two adjacent resonance notches merge into one. Such type of variation in resonance spectrum can be utilized for reconfigurable notch filters. For example, when the tuning power is 0.168 mW (Fig. 6(b)),

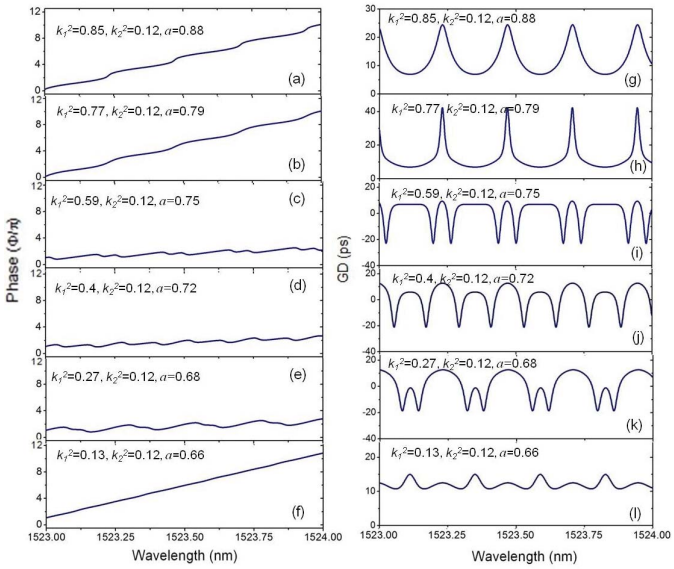

Fig. 7. (a)–(f) Modeled phase spectra of the tunable MZI-based SCOW resonator. (g)–(l) Corresponding GD spectra.

the spectrum exhibits a 20 dB notch at 1523.7 nm, indicating the high rejection of this particular wavelength channel. When the tuning power is increased to 0.722 mW (Fig. 6(e)), then the original notch turns into a peak with a high transmission for the 1523.7 nm wavelength channel. In this way, the stopband and passband can be flipped simply by tuning the MZI couplers.

Fig. 6(g)-(l) show the theoretical modeling of the transmission spectra corresponding to various coupling coefficients and loss factors. Without tuning, the coupling coefficients of two MZI couplers are extracted to be $\kappa_1^2 = 0.85$ and $\kappa_2^2 = 0.12$, although we designed them to be identical and close to unit. We attribute this discrepancy to fabrication induced phase errors in the MZI couplers. As the tuning power increases, the power coupling coefficient κ_1^2 reduces from 0.85 to 0.13 as expected, while κ_2^2 remains unchanged. The associated loss factor a decreases from 0.88 to 0.66 due to the free-carrier induced absorption loss. We note that thermo-optic effect could also be used for coupling coefficient tuning where no extra loss is incurred.

The corresponding modeled phase and group delay spectra of the tunable SCOW resonator are shown in Fig. 7(a)–(l).

Although the active SCOW resonator becomes larger in size after introducing the MZI couplers, it provides a way to conveniently tune the transmission spectrum from single-channel to dual-channel and to broad stopband notches. It should be noted that, if the resonator loss is further lowered by reducing the waveguide scattering loss, the resonance notches and their evolution are more pronounced in the transmission spectrum, making the active SCOW resonator useful in reconfigurable notch filters.

IV. Conclusion

We experimentally demonstrated SCOW resonators and explored the dependence of resonance spectrum on coupling coefficients of the two couplers. SCOW resonators with symmetric couplers exhibit a single-channel stopband under strong coupling and dual-channel stopbands under weak coupling. For SCOW resonators with asymmetric couplers, it exhibits a sharp or a broadened resonance notch An electrically tunable SCOW resonator with couplers made up of 2×2 MZIs was also demonstrated. The resonance spectrum shows a similar evolution trend with the coupling coefficient. Theoretical modeling based on the transfer matrix approach well explains the experimental results.

References

[1] G. T. Reed, *Silicon Photonics: The State of the Art*. New York, NY, USA: Wiley, 2008.

[2] L. Zhou and A. W. Poon, "Electrically reconfigurable silicon microring resonator-based filter with waveguide coupled feedback," *Opt. Express*, vol. 15, no. 15, pp. 9194–9204, Jul. 2007.

[3] P. Dong, *et al.*, "GHz-bandwidth optical filters based on high-order silicon ring resonators," *Opt. Express*, vol. 18, no. 23, pp. 23784–23789, Nov. 2010.

[4] I. White, H. Oveys, X. Fan, T. Smith, and J. Zhang, "Integrated multiplexed biosensors based on liquid core optical ring resonators and antiresonant reflecting optical waveguides," *Appl. Phys. Lett.*, vol. 89, no. 19, p. 191106-1–191106-3, Nov. 2006.

[5] K. De Vos, I. Bartolozzi, E. Schacht, P. Bienstman, and R. Baets, "Silicon-on-insulator microring resonator for sensitive and label-free biosensing," *Opt. Express*, vol. 15, no. 12, pp. 7610–7615, Jun. 2007.

[6] B. Lee, B. Small, K. Bergman, Q. Xu, and M. Lipson, "Transmission of high-data-rate optical signals through a micrometer-scale silicon ring resonator," *Opt. Lett.*, vol. 31, no. 18, pp. 2701–2703, Sep. 2006.

[7] F. Liu, Q. Li, Z. Zhang, M. Qiu, and Y. Su, "Optically tunable delay line in silicon microring resonator based on thermal nonlinear effect," *IEEE J. Sel. Topics Quantum Electron.*, vol. 14, no. 3, pp. 706–712, May/Jun. 2008.

[8] Q. Li, Z. Zhang, J. Wang, M. Qiu, and Y. Su, "Fast light in silicon ring resonator with resonance-splitting," *Opt. Express*, vol. 17, no. 2, pp. 933–940, Jan. 2009.

[9] Z. Zhang, M. Dainese, L. Wosinski, and M. Qiu, "Resonance-splitting and enhanced notch depth in SOI ring resonators with mutual mode coupling," *Opt. Express*, vol. 6, no. 7, pp. 4621–4630, Mar. 2008.

[10] L. Y. Mario and M. K. Chin, "Optical buffer with higher delay-bandwidth product in a two-ring system," *Opt. Express*, vol. 16, no. 3, pp. 1796–1807, Feb. 2008.

[11] L. Zhou, T. Ye, and J. Chen, "Coherent interference induced transparency in self-coupled optical waveguide based resonators," *Opt. Lett.*, vol. 36, no. 1, pp. 13–15, Jan. 2011.

[12] L. Zhou, J. Chen, X. Sun, J. Xie, and H. Zhu, "Optical signal processing using silicon resonance and slow-light structures," *Proc. SPIE*, vol. 8266, pp. 82660N-1–82660N-9, Feb. 2012.

[13] X. Sun, *et al.*, "Experimental demonstration of self-coupled optical waveguide (SCOW) based resonators," in *Proc. 17th Opto-Electron. Commun. Conf.*, Jul. 2012, pp. 541–542.

[14] K. K. Lee, D. R. Lim, L. C. Kimerling, J. Shin, and F. Cerrina, "Fabrication of ultralow-loss Si/SiO_2 waveguide by roughness reduction," *Opt. Lett.*, vol. 26, no. 23, pp. 1888–1890, Dec. 2001.